Title:

Cell-Type-Specific Decrease of the Intrinsic Excitability of Motor Cortical Pyramidal Neurons in Parkinsonism

Abbreviated title:

Decreased Intrinsic Excitability of Motor Cortical Pyramidal Neurons in Parkinsonism

Authors: Liqiang Chen, Samuel Daniels, Yerim Kim, Hong-Yuan Chu

Affiliation: Department of Neurodegenerative Science, Van Andel Institute

Address: 333 Bostwick Ave, N.E., Grand Rapids, MI 49503

Correspondence: Hong-Yuan Chu, Ph.D., email: hongyuan.chu@vai.org

Number of pages: 42

Number of figures: 8

Number of words for Abstract: 239

Number of words for Introduction: 573

Number of words for Discussion: 1174

Conflict of interest: The authors declare no competing financial interests.

Acknowledgements: This work was supported by NINDS grant R01NS121371 and the startup fund from Van Andel Institute (H.Y.C). The authors thank Mr. David Nadziejka for technical editing.

Abstract

The hypokinetic motor symptoms of Parkinson's disease (PD) are closely linked with a decreased motor cortical output as a consequence of elevated basal ganglia inhibition. However, whether and how the loss of dopamine alters the cellular properties of motor cortical neurons in PD remains undefined. We induced parkinsonism in adult C57BL6 mice of both sexes by injecting neurotoxin, 6-hydroxydopamine, into the medial forebrain bundle. By using *ex vivo* patch-clamp recording and retrograde tracing approach, we found that the intrinsic excitability of pyramidal tract neurons (PTNs) in the motor cortical layer 5b was greatly decreased in parkinsonism; but the intratelencephalic neurons (ITNs) were not affected. The cell-type-specific intrinsic adaptations were associated with a depolarized threshold and broadened width of action potentials in PTNs. Moreover, the loss of midbrain dopaminergic neurons impaired the capability of M1 PTNs to sustain high-frequency firing, which could underlie their abnormal pattern of activity in the parkinsonian state. We also showed that the decreased excitability in parkinsonism was caused by an impaired function of both persistent sodium channels and the large conductance, Ca^{2+}-activated K^{+} channels. Acute activation of dopaminergic receptors failed to rescue the impaired intrinsic excitability of M1 PTNs in parkinsonian mice. Altogether, our data demonstrated a cell-type-specific decrease of the excitability of M1 pyramidal neurons in parkinsonism. Thus, intrinsic adaptations in the motor cortex, together with pathological basal ganglia inhibition, underlie the decreased motor cortical output in parkinsonian state and exacerbate parkinsonian motor deficits.

42 **Significance statement**

43 The degeneration of midbrain dopaminergic neurons in Parkinson's disease remodels
44 the connectivity and function of cortico–basal ganglia–thalamocortical network.
45 However, whether and how dopaminergic degeneration and the associated basal
46 ganglia dysfunction alter motor cortical circuitry remain undefined. We found that
47 pyramidal neurons in the layer 5b of the primary motor cortex (M1) exhibit distinct
48 adaptations in response to the loss of midbrain dopaminergic neurons, depending on
49 their long-range projections. Besides the decreased thalamocortical synaptic excitation
50 as proposed by the classical model of Parkinson's pathophysiology, these results, for
51 the first time, show novel cellular and molecular mechanisms underlying the abnormal
52 motor cortical output in parkinsonism.

53

Introduction

The degeneration of dopamine (DA) neurons in the substantia nigra (SN) alters the connection and computation of cortico–basal ganglia–thalamocortical network, which underlies the devastating motor symptoms in Parkinson's disease (PD), including akinesia, bradykinesia, and rigidity (Albin et al., 1989; Galvan and Wichmann, 2008; McGregor and Nelson, 2019). Specially, the loss of SN DA neurons increases and decreases the activities of indirect and direct pathways, respectively, which disrupts the balanced activity between striatal direct and indirect pathways, leading to the hypokinetic symptoms in PD (Albin et al., 1989; DeLong, 1990). The pathway-specific alterations in the striatum following the loss of SN DA neurons induce numerous cellular and synaptic changes in the basal ganglia nuclei and extended brain regions, which further drive the abnormal neural activity throughout the cortico–basal ganglia–thalamocortical network in parkinsonism (Gittis et al., 2011; Kita and Kita, 2011; Fieblinger et al., 2014; Chu et al., 2015, 2017; Mathai et al., 2015; Shen et al., 2015; Parker et al., 2016, 2018; Sharott et al., 2017; McIver et al., 2019; Willard et al., 2019).

The primary motor cortex (M1) plays essential and complex roles in motor control and motor learning and is a key node in the cortico–basal ganglia–thalamocortical network (Shepherd, 2013; Ebbesen and Brecht, 2017; Ebbesen et al., 2018). M1 is a laminar structure and contains a heterogeneous group of neurons that differ in gene expression, morphology, connectivity, and electrophysiological properties (Sheets et al., 2011; Oswald et al., 2013; Shepherd, 2013; Suter et al., 2013; Economo et al., 2018). These neurons can be classified into the intratelencephalic neurons (ITNs) distributed across the layers (L) 2-6 and the pyramidal tract neurons (PTNs) that mainly locate within the L5b (Oswald et al.,

134 2013; Shepherd, 2013). Both PTNs and ITNs project to the striatum and receive basal
135 ganglia feedbacks through the transition of the motor thalamus (Bodor et al., 2008; Kita
136 and Kita, 2011; Kress et al., 2013; Lee et al., 2020). In physiological state, M1 network
137 dynamics plays an essential role in the execution and coordination of complex
138 movements and the acquisition of motor skills (Guo et al., 2015a; Kawai et al., 2015;
139 Sreenivasan et al., 2016; Barthas and Kwan, 2017; Ebbesen et al., 2017; Wang et al., 2017;
140 Economo et al., 2018; Sauerbrei et al., 2020). In parkinsonian state, M1 exhibits an aberrant
141 oscillation and bursting pattern of activity at both individual neuron and population levels
142 (Goldberg et al., 2002; Mallet et al., 2008; Pasquereau and Turner, 2011; Shimamoto et al.,
143 2013; Hemptinne et al., 2015; Pasquereau et al., 2016), which disrupt its normal function in
144 motor control and motor learning.

145 The abnormal neuronal activity in the M1 has been hypothesized to be a
146 consequence of pathological basal ganglia output (Hosp et al., 2011, 2015; Pasquereau and
147 Turner, 2011; Guo et al., 2015b; Pasquereau et al., 2016), but the cellular adaptations could
148 also play a role in such abnormal activities. Moreover, compelling evidence suggests
149 that PTNs and ITNs adapt differently to the degeneration of midbrain DA neurons
150 (Pasquereau and Turner, 2011; Pasquereau et al., 2016).Yet, the cellular and synaptic
151 mechanisms of such adaptations remain unknown. We hypothesized that loss of SN DA
152 neurons alters the intrinsic properties of M1 pyramidal neurons in a cell-type-specific
153 manner, which can contribute to the abnormal neuronal activity of M1 in parkinsonism.
154 We addressed these hypotheses using electrophysiology and retrograde tracing
155 approach in mice with 6-hydroxydopamine (6-OHDA) lesion, an established model of
156 parkinsonism.

Material and Methods

Animals

Adult (3–4 months old) C57BL/6 mice of both sexes were used in the study. Mice were housed up to four animals per cage under a 12-h light/12-h dark cycle with access to food and water *ad libitum* in accordance with Van Andel Institute IACUC and NIH guidelines for care and use of animals. All the animal experiments were reviewed and approved by IACUC at Van Andel Institute.

Stereotaxic surgery

Mice, under 2% isoflurane anesthesia, were placed in a stereotaxic frame (Kopf), and were supported by a thermostatic heating pad. To induce degeneration of SN DA neurons, 6-OHDA (3–4 mg/mL, 1.0 μL) was injected unilaterally into the medial forebrain bundle (MFB, from bregma (in mm): anteroposterior, -0.7, mediolateral, +1.2, dorsoventral, -4.7) over 10 min using a 10-μl syringe (Hamilton) and a motorized microinjector (Stoelting, Wood Dale, IL, USA) (Chu et al., 2017). Controls were injected in the same location with vehicle. Desipramine (25 mg/kg) and pargyline (50 mg/kg) were subcutaneously injected 30–40 min prior to 6-OHDA injection, to enhance the toxicity of 6-OHDA on dopaminergic neurons and reduce damages to noradrenergic system (Chu et al., 2015, 2017). To label and identify PTNs and ITNs in the M1, animals also received red or green Retrobeads (0.3 μL, Lumafluor Inc) injected into the ipsilateral pontine nuclei (from bregma (in mm): anteroposterior, -5.0; mediolateral, +0.6; dorsoventral, -5.0; 0.3 μl per injection) or the contralateral dorsolateral striatum (from bregma (in mm):

218 anteroposterior, +0.4; mediolateral, -2.0; dorsoventral, -2.8). The surgical wound was
219 closed using sutures and mice were allowed to recover after surgery in a heated cage
220 with access to food and water at the cage-floor level. Coronal brain sections containing
221 the forelimb region of M1 from 6-OHDA- or vehicle-injected mice were prepared 3-4
222 weeks after surgery for *ex vivo* electrophysiology.
223
224 **Slice preparation**
225 Mice were deeply anesthetized with intraperitoneal avertin (250–300 mg/kg) and then
226 were perfused transcardially with ice-cold, sucrose-based, artificial cerebrospinal fluid
227 (aCSF) containing (in mM) 230 sucrose, 26 $NaHCO_3$, 10 glucose, 10 $MgSO_4$, 2.5 KCl,
228 1.25 NaH_2PO_4, and 0.5 $CaCl_2$. Next, coronal brain slices (250 μm) containing M1
229 forelimb regions were prepared in the same slicing solution using a vibratome
230 (VT1200S; Leica Microsystems Inc., Buffalo Grove, IL, USA). Brain slices were kept in
231 normal aCSF (in mM: 126 NaCl, 26 $NaHCO_3$, 10 glucose, 2.5 KCl, 2 $CaCl_2$, 2 $MgSO_4$,
232 1.25 NaH_2PO_4, 1 sodium pyruvate and 0.005 L-glutathione) equilibrated with 95% O_2
233 and 5% CO_2 for 30 min at 35 °C and then held at room temperature for 30 min.
234 Electrophysiological recordings started after this 1-hour recovery period.
235
236 ***Ex vivo* electrophysiology recording**
237 Brain slices were transferred into a recording chamber perfused at a rate of 4 mL/min
238 with synthetic interstitial fluid (in mM: 126 NaCl, 26 $NaHCO_3$, 10 glucose, 3 KCl, 1.6
239 $CaCl_2$, 1.5 $MgSO_4$, 1.25 NaH_2PO_4) equilibrated with 95% O_2 and 5% CO_2 at 35 °C via a
240 feedback-controlled in-line heater (TC-324C, Warner Instruments). DNQX (20 μM), D-

241 APV (50 μM), and SR-95531 (10 μM) were routinely added to block synaptic
242 transmission mediated by ionotropic glutamatergic and GABAergic receptors. Neurons
243 were visualized and recorded under gradient contrast SliceScope 6000 (Scientifica, UK)
244 with infrared illumination using a CCD camera (SciCam Pro, Scientifica, UK) and
245 motorized micromanipulators (Scientifica, UK). Individual neurons labeled with
246 Retrobeads in the M1 L5b were identified using a 60X water immersion objective lens
247 (Olympus, Japan) and targeted for whole-cell patch-clamp recording, using a
248 MultiClamp 700B amplifier and a Digidata 1550B digitizer under the control of
249 pClamp11 (Molecular Devices, San Jose, USA). Data were collected at a sampling rate
250 of 20-50 KHz. Borosilicate glass pipettes (O.D. = 1.5 mm, I.D. = 0.86 mm, item#:
251 BF150-86-10, Sutter Instruments, Novato, CA) for patch clamp recordings (4–7 MΩ)
252 were pulled using a micropipette puller (P1000, Sutter Instruments, Novato, CA). Pipette
253 capacitance was compensated for before the formation of the whole-cell configuration.
254 Series resistance (Rs) was regularly monitored and compensated for with the bridge
255 balance circuit in current clamp mode. Liquid junction potential (about 11 mV) was
256 corrected. Under current clamp mode, pipette capacitance was neutralized using
257 MultiClamp 700B amplifier. Briefly, ~10 mV sawtooth pattern of voltage trace was
258 generated through “tuning” function. Then, the degree of capacitance neutralization was
259 determined by gradually increasing capacitance values until voltage oscillations were
260 about to onset.

261 Retrobeads-labeled neurons in the L5b of M1 were recorded in whole-cell
262 current-clamp mode to study their intrinsic properties. In these experiments, glass
263 pipettes were filled with a potassium gluconate-based internal solution of (in mM) 140 K-

287 gluconate, 3.8 NaCl, 1 $MgCl_2$, 10 HEPES, 0.1 Na_4-EGTA, 2 ATP-Mg, and 0.1 GTP-Na,
288 pH 7.3, osmolarity 290 mOsm. The resting membrane potential (V_m) was recorded once
289 the whole-cell configuration was obtained. The intrinsic properties and excitability of M1
290 pyramidal neuron subtypes were studied by injecting a family of current steps ranging
291 from -240 pA to 720 pA in 40-pA increments and with a duration of 1 s. Current
292 injections were from V_m and no additional holding current was injected. Input resistance
293 (R_m) was determined by measuring the steady-state voltage responses to a series of 1-
294 s hyperpolarizing currents, as the slope of linear fit to the resulting voltage-current
295 relationship. The membrane time constant (τ_m) was determined as the slow component
296 of a double-exponential fit of the voltage decays in response to -40 or -80 pA, 1-s
297 current injections (i.e., a 5–10 mV voltage change). Cell capacitance (C_m) was derived
298 from the equation $C_m = \tau_m / R_m$.

299 The rheobase, as an indicator of neuronal excitability, was defined as the current
300 intensity to elicit an action potential (AP). Rheobase was determined by first probing the
301 response of neurons to 1-s current injections to define the targeted range of current
302 intensities, and then by bounding the rheobase through small current steps (1 pA
303 increments). AP waveforms at the rheobase were systematically analyzed and
304 quantified using Clampfit 11.1. Specifically, the threshold of AP was determined as the
305 voltage level at which d*V*/d*t* exceeded 20 mV/ms. AP amplitude was defined as the
306 voltage difference between the threshold and the peak voltage. AP half-width was
307 measured as the time difference at 50% of AP amplitude. Fast afterhyperpolarizations
308 (fAHPs) were measured as the negative voltage peaks relative to the threshold within
309 2–5 ms from AP threshold (Villalobos et al., 2004; Bean, 2007). To quantify spike trains,

312 spike frequency adaptation was measured as the ratio between the last inter-spike-
313 interval and the average of the first two inter-spike-intervals. The gain of the spike-
314 current curve was defined as the slope of the linear portion of the instantaneous spike-
315 current curve.
316
317 **Immunohistochemistry**
318 Immunoreactivity of tyrosine hydroxylase (TH) and norepinephrine transporter (NET)
319 was assessed to validate the degeneration of the nigrostriatal DA projections and
320 noradrenergic projections to M1 in 6-OHDA-injected mice. Briefly, brain tissues were
321 first fixed in 4% paraformaldehyde in 0.1 M phosphate buffer, pH7.4, at 4 °C for 12
322 hours before rinsing in phosphate-buffered saline (PBS, 0.05 M; pH 7.4). Tissues was
323 re-sectioned at 70 μm using a vibratome (Leica VT1000S; Microsystems Inc.).
324 Immunochemical detection of TH was conducted in PBS containing 0.2% Triton X-100
325 (Fisher Scientific) and 2% normal donkey serum (Sigma-Aldrich, St. Louis, MO). Brain
326 sections were incubated in primary antibody (mouse anti-TH antibody, 1:2000, cat#:
327 MAB318, Sigma-Aldrich, St. Louis, MO, USA; or mouse anti-NET antibody, 1:1000, cat#
328 211463, Abcam, Cambridge, MA, USA) for 48 h at 4 °C or overnight at room
329 temperature (RT), washed in PBS, and then incubated in the secondary antibody
330 (donkey anti-mouse Alexa Fluor 488, cat#: 715-545-150 or donkey anti-mouse Alexa
331 Fluor 594, cat#715-585-150; 1: 500, Jackson ImmunoReseach, West Grove, PA, USA)
332 for 90 minutes at RT before washing with PBS. Brain sections were mounted on glass
333 slides using VECTASHIELD antifade mounting medium (cat#: H-1000, Vector
334 Laboratories, Burlingame, CA, USA) and were cover-slipped. TH immunoreactivity in

358 the dorsal striatum and the overlying motor cortex in the same section was imaged
359 using an Olympus BX63F microscope equipped with an Olympus DP80 camera or a
360 confocal laser scanning microscope (A1R; Nikon, Melville, USA). TH immunoreactivity
361 of each section was determined as the difference between the immunofluorescence
362 between the dorsal striatum and the motor cortex (Chu et al., 2015). The intensity of TH
363 and NET immunofluorescence was quantified using ImageJ (NIH, Bethesda, MD, USA).
364

365 **Animal Behavior**

366 To validate the development of parkinsonian bradykinesia and akinesia prior to
367 electrophysiology studies, vehicle- and 6-OHDA-injected mice were subject to 1) open
368 field locomotion test for 10 min and their locomotor activity as well as rotations were
369 monitored and quantified using Anymaze software (Stoelting, Wood Dale, IL); 2)
370 cylinder test to assess their spontaneous forelimbs use during weight-bearing touch on
371 wall of a 600 ml glass cylinder. Spontaneous exploration of mice was recorded using an
372 HD digital camcorder at 60 fps (Panasonic, HC-V180K) and analyzed off-line by a
373 researcher blinded to treatments.
374

375 **Experimental design and statistical analysis**

376 Data were analyzed in Clampfit 11.1 (Molecular Devices, San Jose, CA) and ImageJ
377 (NIH). Statistics were done using Prism8 (GraphPad Software, San Diego, CA, USA).
378 To minimize the assumption of the data normality, we used non-parametric, distribution-
379 independent Mann-Whiney U (MWU) or Wilcoxon signed rank (WSR) tests for non-
380 paired or paired data comparisons, respectively. The Holm-Bonferroni correction was

applied for multiple comparisons. All tests were two-tailed, and an α-level of 0.05 was used to determine statistical significance. Results are reported as median and interquartile range. Boxplots illustrate the median (central line), interquartile range (box), and 10–90% range (whiskers) of data. Data are available upon request.

410 **Results**

411 All physiology studies were conducted between 3- and 4-weeks post-surgery, when the
412 level of midbrain DA degeneration and functional adaptations in the brain have reached
413 maximum and been stabilized (Vila et al., 2000; Viaro et al., 2011). At 3 weeks post-
414 surgery, mice with 6-OHDA lesion (hereinafter, "6-OHDA mice") showed featured
415 parkinsonians akinesia and bradykinesia versus vehicle-injected controls (hereinafter,
416 "controls"), as supported by 1) a reduced travelled distance in open-field locomotion test
417 (6-OHDA mice = 18 [16, 22] m, controls = 41 [32, 50] m, n = 13 mice from each group, p
418 < 0.0001, MWU); 2) ipsilateral rotations (%ipsilateral rotations, 6-OHDA mice = 100 [97,
419 100]%, controls = 41 [26, 53]%, n = 13 mice from each group, p < 0.0001, MWU); and
420 3) impaired forelimb use (%ipsilateral forelimb use: 6-OHDA mice = 88 [83, 92]%,
421 controls = 50 [49, 53]%, n = 13 mice from each group, p < 0.0001, MWU). In *post hoc*
422 histology studies, 6-OHDA mice showed > 80% reduction of striatal TH
423 immunoreactivity (TH-ir) in the hemisphere with lesion (%TH-ir in the ipsilateral versus
424 the contralateral striatum, 6-OHDA mice = 0 [0, 0]%, and controls = 97 [85, 102]%, n =
425 16 mice for each group). In addition, desipramine was routinely administered to inhibit
426 reuptake of 6-OHDA by noradrenergic terminals. Given the heavy noradrenergic
427 innervation of the cortical regions, we therefore validated the effect of desipramine by
428 immunostaining of cortical NET and striatal TH in a separate cohort of animals. %NET-ir
429 in the ipsi- versus contra-lateral L5 of M1, 6-OHDA = 92 [78, 108]%, while %TH-ir in the
430 ipsi- versus contra-lateral striatum = 0 [0, 3.5]%, n = 8 sections/4 mice.

431

434 **Cell-type-specific decrease in the intrinsic excitability of M1 L5b pyramidal**
435 **neurons following the loss of midbrain DA neurons.**
436 We compared the intrinsic excitability of projection-defined pyramidal neurons in the L5b
437 of M1 from controls and 6-OHDA mice. To identify M1 pyramidal neurons based on
438 long-range projections, Retrobeads were stereotaxically injected into the ipsilateral
439 pontine nuclei (Figure 1A) and the contralateral striatum (Figure 2A) to retrogradely
440 label PTNs (Figure 1B) and ITNs (Figure 2B), respectively. The intrinsic
441 electrophysiological properties of M1 PTNs and ITNs were assessed using whole-cell
442 current-clamp recording in the presence of antagonists of ionotropic glutamatergic and
443 GABAergic receptors, including DNQX (20 μM), D-APV (50 μM), and SR95531 (10 μM).
444 The intrinsic excitability of M1 pyramidal neuron subtypes was assessed by
445 somatic injection of a range of depolarizing currents from V_m in controls and 6-OHDA
446 mice (Figures 1C, D). First, the intensity of somatic current injection to elicit single
447 action potential (AP) increased significantly for PTNs from 6-OHDA mice relative to
448 controls (rheobase, control = 126 [80, 220] pA), n = 39 neurons/4 mice, 6-OHDA = 175
449 [120, 250] pA, n = 30 neurons/3 mice, p = 0.03, MWU, Figure 1E). Moreover, the gain of
450 spike-current curve decreased significantly in M1 PTNs from 6-OHDA mice relative to
451 controls (control = 97 [95, 98] Hz/nA, n = 39 neurons/4 mice; 6-OHDA = 62 [44, 73]
452 Hz/nA, n = 30 neurons/3 mice; p < 0.0001, MWU; Figure 1F). The same reduction was
453 also detected for the maximal spike frequency (e.g., frequency at 720 pA current
454 injection, control = 47 [39, 57] Hz, n = 39 neurons/4 mice; 6-OHDA = 38 [23, 45] Hz, n =
455 30 neurons/3 mice; p = 0.0002, MWU; Figure 1G). M1 PTNs could sustain persistent
456 firing with minimal spike adaptation during repetitive firing in the physiological state

(Figure 1C) (Oswald et al., 2013; Suter et al., 2013). However, PTNs showed significantly enhanced spike adaptation in 6-OHDA mice (Figure 1 C). The spike adaptation of a 10-Hz spike train, control = 1.2 [1.0, 1.6], n = 39 neurons/4 mice; 6-OHDA = 1.6 [1.3, 2.3], n = 30 neurons/3 mice; p = 0.0011, MWU (Figures 1C, H). Altogether, these results suggest a significant reduction in the intrinsic excitability of M1 PTNs in parkinsonism.

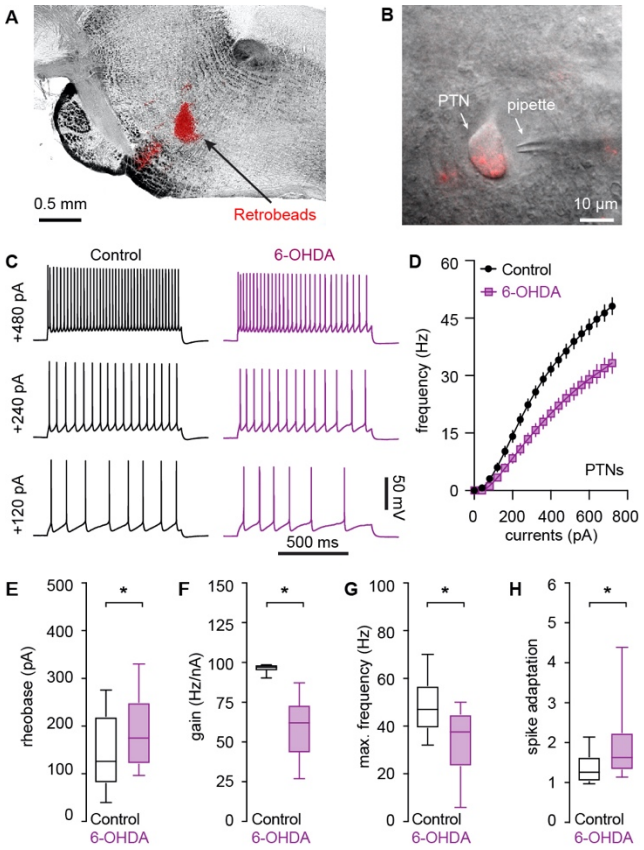

Figure 1. Decreased intrinsic excitability of PTNs in the L5b of M1 following the loss of midbrain DA neurons. A and B) Representative graphs showing the injection site of red Retrobeads in the pontine nuclei (**A**) and a retrogradely labeled PTN in L5b of M1 (**B**). **C and D**) Representative spike trains of PTNs evoked by somatic current injections from controls and 6-OHDA mice (**C**), and the frequency-current relationship of the PTNs from controls and 6-OHDA mice (**D**). **E-H**) Summarized results showing an increased rheobase (**E**), a reduced gain of spike-current curve (**F**), a decreased firing frequency in response to maximal current injections (i.e., 720 pA) (**G**), and an enhanced spike adaptation (**H**) in PTNs from 6-OHDA mice relative to those from controls. *, p < 0.05, MWU.

In contrast, M1 ITNs from controls and 6-OHDA mice showed comparable intrinsic excitability (Figure 2). This was reflected by four measures, namely, a) similar rheobase (control = 155 [118, 213] pA, 6-OHDA = 184 [79, 252] pA, n = 30 neurons/3 mice for each group, p = 0.4, MWU, Figure 2E); b) the unaltered gain of spike-current

curve (control = 84 [61, 94] Hz/nA, 6-OHDA = 74 [61, 89] Hz/nA, n= 30 neurons/3 mice for each group; p = 0.3, MWU; Figure 2F); c) the maximal spike frequency (control = 53 [38, 64] Hz, 6-OHDA = 45 [35, 60] Hz, n = 30 neurons/3 mice for each group; p = 0.15, MWU; Figure 2D, G); and d) spike adaptations (control = 1.6 [1.3, 2.2], 6-OHDA = 1.9 [1.3, 2.4], n = 30 neurons/3 mice for each group; p = 0.39, MWU; Figure 2C, H). Altogether, our results thus suggest that the M1 L5b pyramidal neurons exhibited cell-type-specific decrease of intrinsic excitability in parkinsonism.

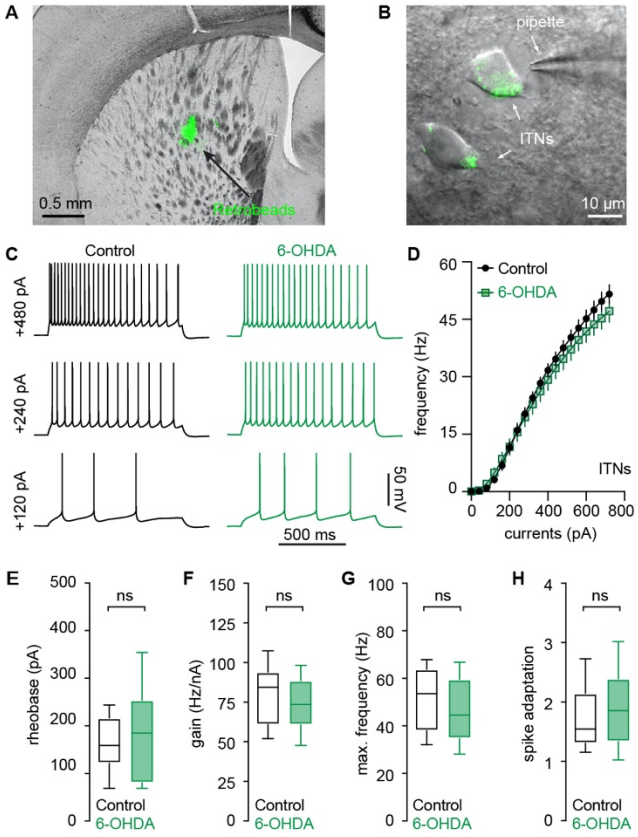

Figure 2. Intact intrinsic excitability of ITNs in the M1 L5b following the loss of midbrain DA neurons. A and B) Representative graphs showing the injection site of green Retrobeads in the dorsal striatum (**A**) and retrogradely labeled M1 L5b ITNs (**B**). **C and D**) Representative spikes trains evoked by somatic current injections into ITNs from control and 6-OHDA mice (**C**), and the frequency-current relationship of ITNs from controls and 6-OHDA mice (**D**). **E-H**) Boxplots showing a similar rheobase (**E**), an unaltered gain of spike-current curve (**F**), firing frequency in response to maximal current injections (i.e., 720 pA) (**G**), and spike adaptation (**H**) between ITNs from 6-OHDA mice and controls. ns, not significant, MWU.

No change in the passive membrane properties of M1 L5b pyramidal neurons following the loss of midbrain DA neurons.

Next, we determined whether alterations in the passive membrane properties contribute to the difference in the intrinsic excitability of M1 PTNs and ITNs in parkinsonism. In the

presence of antagonists of fast ionotropic glutamatergic and GABAergic receptors, PTNs in 6-OHDA mice and controls had similar resting membrane potential (V_m, control = -75.8 [-77.2, -74.9] mV, n = 39 neurons/4 mice; 6-OHDA = -76.1 [-77.1, -74.9] mV, n= 30 neurons/3 mice; p = 0.87, MWU, Figure 3A) and input resistance (R_m, control = 72.9 [60, 83.8] MΩ, n = 39 neurons/4 mice; 6-OHDA = 71.3 [64, 86.6] MΩ, n= 30 neurons/3 mice; p = 0.91, MWU, Figure 3B). In addition, PTNs from 6-OHDA mice did not show changes in their cell capacitance (C_m) and membrane time constant (τ_m) relative to those from controls (C_m, control = 212 [160, 239] pF, n = 39 neurons/4 mice, 6-OHDA = 192 [167, 268] pF, n = 30 neurons/3 mice, p = 0.7, MWU, Figure 3C; τ_m, control = 19.4 [14.4, 23.4] ms, n = 39 neurons/4 mice, 6-OHDA = 20.9 [12.4, 30.5] ms, n = 30 neurons/3 mice, p = 0.5, MWU, Figure 3D).

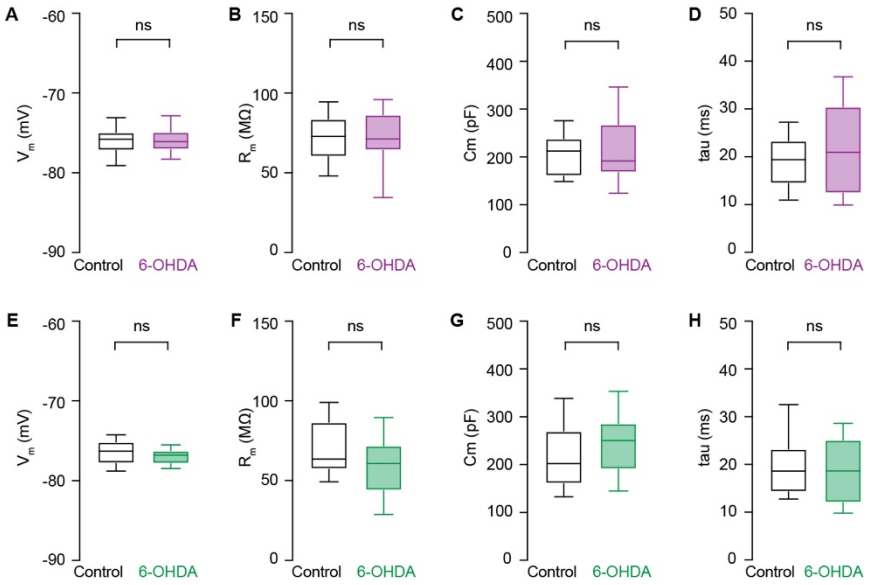

529

Figure 3. No change in the passive membrane properties of PTNs and ITNs in the M1 L5b following the loss of midbrain DA neurons. A-D) Boxplots showing no changes in the resting membrane potential (**A**), input resistance (**B**), cell capacitance (**C**), and time constant (**D**) of PTNs from 6-OHDA mice relative to those from controls. **E-H**) Similar measures of passive membrane properties of ITNs from controls and 6-OHDA mice. ns, not significant, MWU.

530 Similarly, ITNs showed comparable passive membrane properties between groups,
531 namely, V_m (control = -76.3 [-77.8, -75.1] mV, 6-OHDA = -76.8 [-77.9, -76.2] mV, n = 30
532 neurons/3 mice for each group, p = 0.2, MWU, Figure 3E), R_m (control = 63.5 [57.1,
533 86.7] MΩ, 6-OHDA = 60.8 [43.8, 72] MΩ, n = 30 neurons/3 mice for each group, p =
534 0.15, MWU, Figure 3F), C_m (control = 202 [160, 270] pF, 6-OHDA = 250 [190, 287] pF,
535 n = 30 neurons/3 mice for each group, p = 0.13, MWU, Figure 3G), and τ_m (control =
536 18.6 [14.2, 23.3] ms, 6-OHDA = 18.6 [12, 25.2] ms, n = 30 neurons/3 mice for each
537 group, p = 0.6, MWU, Figure 3H). Altogether, these results suggest that the cell-type-
538 specific decrease in the excitability of M1 pyramidal neurons is not due to alterations in
539 their passive membrane properties.

540

541 **Cell-type-specific changes in action potential waveforms of M1 L5b pyramidal**
542 **neurons following the loss of midbrain DA neurons.**

543 The shape of the action potential is determined by the interaction of numerous voltage-
544 gated ion channels and has profound effects on the rate and pattern of neuronal firing
545 (Bean, 2007). We therefore analyzed the morphology of AP of PTNs and ITNs at the
546 rheobase from controls and 6-OHDA mice (Figures 4A, H). In parkinsonian animals, M1
547 PTNs showed a depolarized AP threshold (controls = -49.7 [-51.5, -47.7] mV, n = 39
548 neurons/4 mice, 6-OHDA = -47.9 [-50.3, -45.8] mV, n = 30 neurons/3 mice, p = 0.015,

551 MWU, Figure 4B) and a striking AP broadening (AP half-width, controls = 0.69 [0.66,
552 0.75] ms, n = 39 neurons/4 mice; 6-OHDA = 0.77 [0.72, 0.82] ms, n = 30 neurons/3
553 mice; p = 0.0008, MWU, Figure 4C). The broadened AP of PTNs was associated with a
554 significantly prolonged AP rise time (controls = 0.19 [0.18, 0.22] ms, n = 39 neurons/4
555 mice; 6-OHDA = 0.21 [0.2, 0.24] ms, n = 30 neurons/3 mice; p = 0.0024, MWU; Figures
556 4D) and also a prolonged decay time (controls = 0.8 [0.69, 0.84] ms, n = 39 neurons/4
557 mice, 6-OHDA = 0.9 [0.76, 0.97] ms, 30 neurons/3 mice; p = 0.0023, MWU; Figure 4E).
558 In parkinsonian animals, M1 PTNs also exhibited significant decreases in the maximal
559 rates of AP depolarization (the rise rate, controls = 434 [398, 493] mV/ms, n = 39
560 neurons/4 mice, 6-OHDA = 390 [340, 443] mV/ms, n= 30 neurons/3 mice, p = 0.004,
561 MWU, Figure 4F) and repolarization (the decay rate, controls = -102 [-87, -111] mV/ms,
562 n = 39 neurons/4 mice, and 6-OHDA = -90 [-81, -99] mV/ms, n = 30 neurons/3 mice, p =
563 0.012, MWU, Figure 4G). Thus, the decreased excitability of PTNs in parkinsonism
564 involves impairments in both Na^+ and K^+ conductance that underlies AP depolarization
565 and repolarization, respectively (Bean, 2007).

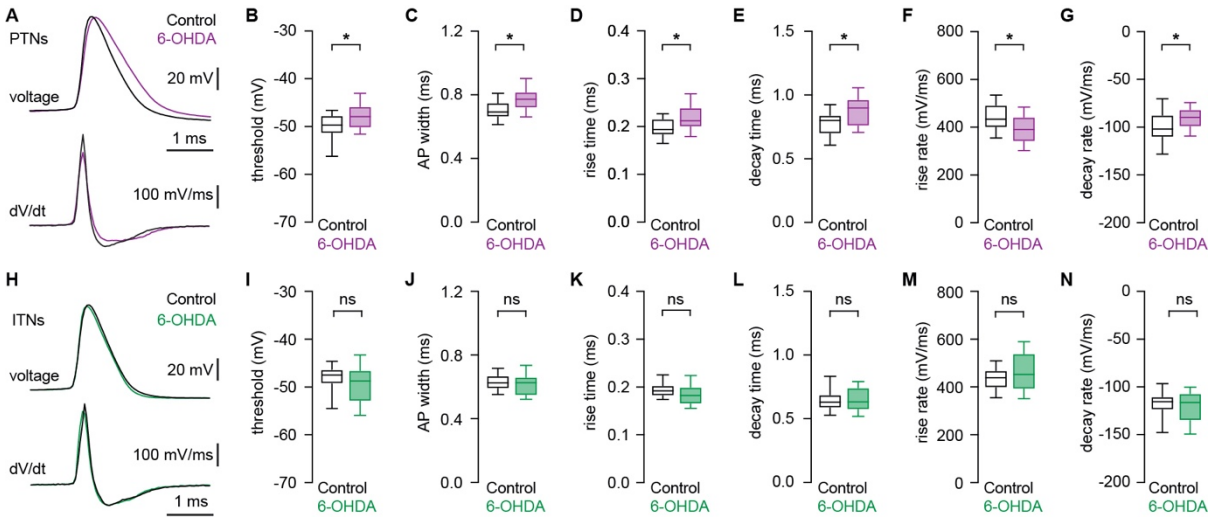

Figure 4. Distinct changes in AP waveforms of PTNs and ITNs in the M1 L5b following loss of midbrain DA neurons. A) **Top**, representative AP waveforms of PTNs from controls and 6-OHDA mice. APs were aligned at threshold and overlaid for comparison. **Bottom**, the corresponding *d*V/*d*t traces plotted against time, showing depolarizing and repolarizing rates of APs. **B and C**) Boxplots showing AP threshold and width of PTNs in 6-OHDA mice and controls. **D and E**), Boxplots showing prolonged AP rise time (**D**) and decay time (**E**) in PTNs from 6-OHDA mice relative to those from controls. **F and G**), Boxplots showing decreased AP rise rate (**F**) and decay rate (**G**) in PTNs from 6-OHDA mice relative to those from controls. **H**) **Top**, representative AP waveforms of ITNs from controls and 6-OHDA mice. APs were aligned at threshold and overlaid for comparison. **Bottom**, the corresponding *d*V/*d*t traces plotted against time, showing depolarizing and repolarizing rates of APs. **I-N**) Boxplot showing similar AP threshold (I) and width (J), rise (K) and decay (L) time, as well as rise (M) and decay (N) rates in ITNs from 6-OHDA mice relative to those from controls. ns, not significant; *, $p < 0.05$, MWU.

In contrast, ITNs from controls and 6-OHDA mice showed unaltered AP threshold (controls = -47.5 [-49.3, -46.3] mV, 6-OHDA = -48.7 [-53, -46.5] mV, n = 30 neurons/3 mice for each group, p = 0.24, MWU, Figure 4I) and AP width (controls = 0.63 [0.59, 0.67] ms; 6-OHDA = 0.63 [0.55, 0.66] ms, n = 30 neurons/3 mice for each group; p = 0.56, MWU; Figure 4J). The similar AP width of ITNs was associated with unaltered time and rates of AP depolarization and repolarization. The rise time was controls = 0.19 [0.18, 0.2] ms, and 6-OHDA = 0.18 [0.16, 0.2] ms (p = 0.13, MWU, Figure 4K). The decay time was controls = 0.63 [0.58, 0.69] ms, and 6-OHDA = 0.63 [0.57, .074] ms (p = 0.94, MWU, Figure 4L). The rise rate values were, controls = 438 [396, 469] mV/ms, and 6-OHDA = 452 [390, 541] mV/ms (p = 0.3, MWU, Figure 4M), and the decay rate

values were, controls = -115 [-110, -124] mV/ms, and 6-OHDA = -116 [-107, -135] mV/ms (p = 0.67, MWU, Figure 4N).

Altogether, these results suggest that disrupted ionic mechanisms for AP generation contribute to cell-type-specific decrease in the intrinsic excitability of PTNs in parkinsonism.

Progressive alterations in AP waveforms of PTNs during repetitive firing following the loss of SN DA neurons.

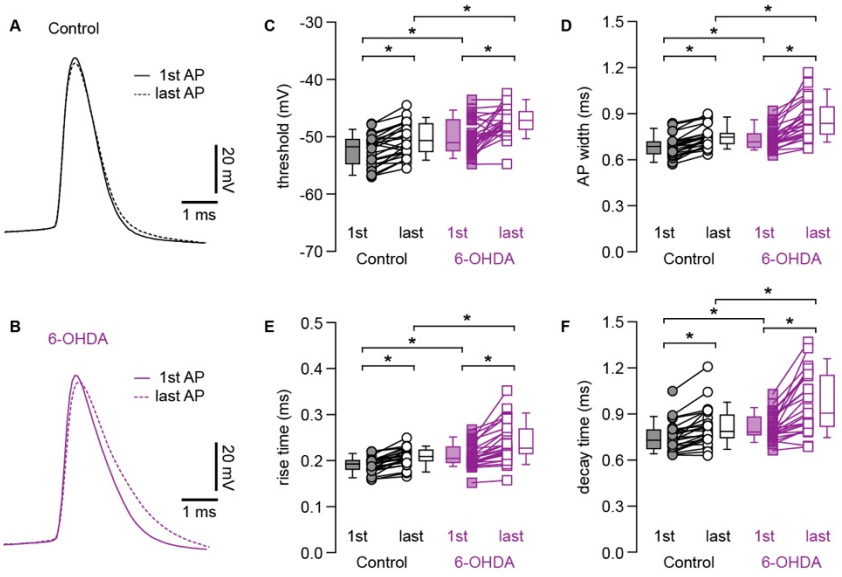

Figure 5. Progressive changes in AP waveforms of M1 PTNs during repetitive firing. **A-B**) The first and the 10th APs from a 10-Hz spike train were superimposed for PTNs from control (**A**) or 6-OHDA mice (**B**). APs were aligned at threshold, and the solid and dashed lines indicated the first and the 10th APs from the spike train, respectively. **C**) Summarized graphs showing the alterations of AP threshold between the first and the 10th APs. Each line connects the AP width of the first and the 10th APs from the same spike train. Box plots indicate the median plus interquartile range of the first and the 10th AP. (**D-F**) Summarized graphs showing changes in AP width (D), rise time (E), and decay time (F) between the first and the 10th APs in PTNs from 6-OHDA mice relative to those from controls. *, $p < 0.05$, WSR or MWU tests.

611 The literature suggests that M1 PTNs are capable to sustain constant AP
612 waveform during repetitive firing (Suter et al., 2013). Thus, we elicited spike trains
613 containing 10 APs from M1 PTNs in controls and 6-OHDA mice and analyzed
614 waveforms of the first and the last APs to study activity-dependent AP modulation
615 during repetitive firing. We noticed a stronger activity-dependent AP waveform
616 modulation in PTNs from 6-OHDA mice relative to those from controls (Figure 5A, B).
617 Specifically, PTNs from both groups exhibited an increased AP threshold during
618 repetitive firing (threshold in controls, 1st AP= -51.8 [-54.8, -50.5] mV, last AP = -50.7 [-
619 52.7, -47.8] mV, n = 25 neurons/5 mice, $p < 0.001$, WSR; threshold in 6-OHDA mice,
620 1st AP = -51 [-52.5, -47.1] mV, last AP = -47.2 [-48.8, -45.6] mV, n= 25 neurons/5 mice,
621 $p < 0.001$, WSR; Figure 5C). Repetitive firing leads to a significantly depolarized
622 threshold of the last APs from 6-OHDA mice relative to those from controls ($p = 0.0003$
623 between groups, MWU, Figure 5C), in addition to the elevated threshold of the 1st APs
624 ($p = 0.02$ between groups, MWU; Figure 5C). This is consistent with activity-dependent
625 inactivation of voltage-dependent transient Na^+ channels (Na_T) during sustained firing
626 (Bean, 2007).
627 APs of PTNs in both controls and 6-OHDA mice also progressively broadened
628 during repetitive firing (AP width in controls, 1st AP = 0.68 [0.64, 0.72] ms, last AP = 0.75
629 [0.7, 0.77] ms, n= 25 neurons/5 mice, $p < 0.0001$, WSR; AP width in 6-OHDA mice, 1st
630 AP = 0.72 [0.68, 0.77] ms, last AP = 0.84 [0.76, 0.94] ms, n= 25 neurons/5 mice, p <
631 0.0001, WSR, Figure 5D). Importantly, repetitive firing led to a significantly broadened
632 last APs in 6-OHDA mice relative to controls (width of the last AP, $p = 0.0004$ between
633 groups, MWU, Figure 5D), in addition to the broadened 1st AP (width of the 1st AP, p =

638 0.01 between groups, MWU, Figure 5D). Moreover, the observed activity-dependent
639 modulation of AP waveforms associated with prolonged rise and decay time in controls
640 and 6-OHDA mice (Figure 5E, F). The values of AP rise time in controls were, the 1st AP
641 = 0.19 [0.18, 0.2] ms, the last AP = 0.21 [0.2, 0.22] ms (n = 25 neurons/5 mice, $p <$
642 0.0001, WSR, Figure 5E) and the values for AP rise time in 6-OHDA mice were, the 1st
643 AP = 0.2 [0.19, 0.23] ms, the last AP = 0.23 [0.21, 0.27] ms (n = 25 neurons/5 mice, $p <$
644 0.0001, WSR, Figure 5E). The rise time of the 1st APs ($p = 0.005$ between groups,
645 MWU, Figure 5F) and last APs ($p = 0.004$ between groups, MWU, Figure 5F) were both
646 significantly increased in 6-OHDA mice relative to those in controls. Similarly, the values
647 of AP decay time in controls were, the first AP = 0.73 [0.67, 0.8] ms, the last AP = 0.79
648 [0.74, 0.89] ms (n = 25 neurons/5 mice, $p < 0.0001$, WSR, Figure 5F). And the values
649 AP decay time in 6-OHDA were, the first AP = 0.78 [0.76, 0.88] ms, the last AP = 0.91
650 [0.82, 1.15] ms (n = 25 neurons/5 mice, $p < 0.0001$, WSR, Figure 5F). The decay time
651 of the 1st APs ($p = 0.01$ between groups, MWU, Figure 5F) and the last APs ($p =0.002$,
652 MWU, Figure 5F) were both significantly increased in 6-OHDA mice relative to those in
653 controls.
654 Altogether, these results suggest that PTNs in parkinsonism show a stronger
655 activity-dependent AP modulation, which, at least partially, leads to a decreased
656 intrinsic excitability.
657
658 **Impaired function of persistent Na^+ currents contributes to the increased**
659 **threshold and decreased intrinsic excitability of PTNs in parkinsonism**
660

683 Persistent sodium current (I_{Nap}) plays an important role in determining AP threshold and
684 its dysfunction contributes to disrupted neuronal activity in several neurological diseases
685 (Bean, 2007; Milescu et al., 2010; Deng and Klyachko, 2016). Given the altered AP
686 threshold and rising phase of APs in 6-OHDA mice (Figure 4B, D, F), we next examined
687 whether I_{Nap} contributes to these alterations. Blockade of I_{Nap} by bath application of low
688 concentration of tetrodotoxin (TTX, 20 nM) (Gage 1998; Deng 2016) significantly
689 elevated the AP threshold at rheobase of PTNs from controls and 6-OHDA mice
690 (controls, baseline = -50.8 [-53.7, -50] mV, TTX = -41.1 [-42.3, -38.2] mV, n = 11
691 neurons/3 mice, p = 0.001, WSR; 6-OHDA, baseline = -48.8 [-49.4, -46.5] mV, TTX = -
692 41.2 [-43.5, -39.4] mV; n = 13 neurons/4 mice, p = 0.0002, WSR, Figure 6A-C). TTX (20
693 nM) also abolished the difference in AP threshold between groups (AP threshold, prior
694 to TTX, p = 0.0018; in TTX, p = 0.5, MWU, Figure 6C). In contrast, blockade of I_{Nap} did
695 not affect AP width at rheobase of PTNs either in controls (baseline = 0.68 [0.61, 0.72]
696 ms, TTX = 0.7 [0.62, 0.82] ms, p = 0.2, WSR, Figure 6D) or in 6-OHDA mice (baseline =
697 0.8 [0.7, 0.81] ms, TTX = 0.77 [0.7, 0.83] ms, p = 0.9, WSR, Figure 6D). With the
698 blockade of I_{Nap}, PTNs from controls and 6-OHDA mice also exhibited activity-
699 dependent increase in AP threshold during repetitive firing of 10 APs (controls in TTX,
700 1st AP = -47.1 [-49.5, -40.7] mV, last AP = -40.9 [-45.8, -38.6] mV, p = 0.004, WSR, n= 9
701 neurons/3 mice; 6-OHDA in TTX, 1st AP = -46.3 [-51.7, -43.1] mV, last AP = -41.4 [-
702 44.8, -35.8] mV, p = 0.0005, WSR, n = 13 neurons/4 mice. Figure 6E). Further, TTX
703 also abolished the difference in AP threshold of both the first and the last APs during
704 repetitive firing (threshold of the first AP, p = 0.65 between groups; threshold of the last

707 AP, p = 0.7 between groups, MWU, Figure 6E). These results indicate disrupted I_{Nap}

708 function underlies the elevated AP threshold in 6-OHDA mice.

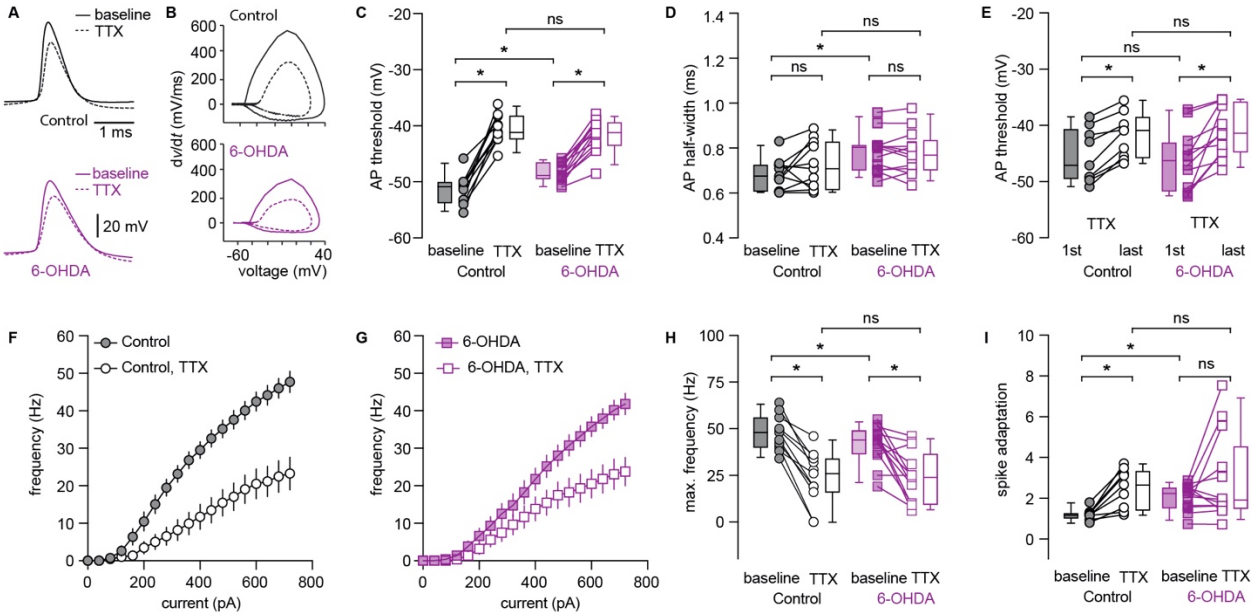

709

Figure 6. Low concentration TTX excludes the decreased intrinsic excitability of PTNs in 6-OHDA mice versus controls. A-B) Representative AP waveforms of PTNs at rheobase from controls (**A**, up) and 6-OHDA mice (**A**, bottom) and the corresponding phase plane plots at baseline and in the presence of TTX (20 nM). **C-D**) Summarized graphs showing changes in AP threshold (**C**) and half-width (**D**) at rheobase in the absence and presence of TTX (20 nM). **E**) Summarized graph showing threshold changes of PTNs from controls and 6-OHDA mice during repetitive firing of 10 APs in the presence of TTX (20 nM). **F-G**) Current-frequency curves of PTNs from controls and 6-OHDA mice in the absence and presence of TTX (20 nM). **H-I**) summarized graphs showing changes in the maximal firing frequency (H) and spike adaptation (**I**) of PTNs from controls and 6-OHDA mice in the absence and presence of TTX (20 nM). *, p < 0.05, n.s., not significant. WSR or MWU tests.

710

711 Next, we tested the hypothesis that a decreased basal I_{Nap} activity exacerbates

712 activity-dependent Na_T inactivation and leads to a decreased excitability of PTNs in 6-

713 OHDA mice. As expected, blockade of I_{Nap} by TTX (20 nM) significantly decreased the

714 number of APs of PTNs from controls and 6-OHDA mice (Figure 6F, G). For example,

715 the maximal number of APs in controls were, baseline = 48 [40, 56], TTX = 26 [16, 34]

716 (n = 11 neurons/3 mice, p = 0.001, WSR, Figure 6H) and in 6-OHDA mice were,

717 baseline = 44 [37, 49], TTX = 24 [10, 37] (n = 13 neurons/4 mice, p = 0.002, WSR,

740 Figure 6H). Importantly, TTX abolished the difference in intrinsic excitability of PTN
741 between groups (AP numbers in TTX between groups, p = 0.96, MWU, Figure 6H).
742 It has been reported that Na_T inactivation contribute to spike adaptation during
743 repetitive firing (Fleidervish et al., 1996; Milescu et al., 2010). Consistently, blockade of
744 I_{Nap} by TTX (20 nM), which promotes Na_T inactivation, dramatically increased spike
745 adaptation in PTNs from controls (adaptation index, baseline = 1.18 [1.0, 1.2], TTX =
746 2.67 [1.43, 3.34], n = 9 neurons/3 mice, p = 0.0039, WSR, Figure 6I), but had little effect
747 to those from 6-OHDA mice (adaptation index, baseline = 2.26 [1.55, 2.53], TTX = 1.93
748 [1.51, 4.55], n = 13 neurons/4 mice, p = 0.34, WSR, Figure 6I). Furthermore, TTX
749 abolished the difference in spike adaptation between groups (controls versus 6-OHDA
750 mice at baseline, p = 0.002; in TTX, p = 1, MWU, Figure 6I).
751 Thus, these data indicated that I_{Nap} dysfunction reduces the availability of Na_T for
752 AP generation and exacerbates their inactivation during repetitive firing, leading to a
753 decreased intrinsic excitability of PTNs in parkinsonism.
754 **Impaired activity of BK channels underlies the broadened APs of M1 PTNs**
755 **following the loss of midbrain DA neurons.**
756 We further examined the ionic mechanisms underlying broadened APs of PTNs in 6-
757 OHDA mice. Following the loss of midbrain DA neurons, the amplitude of the fast
758 afterhyperpolarization (fAHP) in PTNs decreased significantly (controls = 12.5 [10.5,
759 14.3] mV, n = 39 neurons/4 mice; 6-OHDA = 11.2 [10.5, 11.9] mV, n = 30 neurons/3
760 mice; p = 0.036, MWU). These observations suggest that an altered BK channel activity
761 probably underlies the broadened AP of PTNs in 6-OHDA mice, considering its role in

781 AP repolarization, fAHPs, and AP broadening during neuronal repetitive firing in other
782 brain regions (Faber and Sah, 2003; Bean, 2007; Contet et al., 2016).
783 Consistently, the difference in AP width at rheobase of PTNs between groups
784 was abolished by intracellular BAPTA (10 mM, a high-affinity Ca^{2+} chelator) (controls =
785 0.84 [0.79, 0.92] ms, n = 26 neurons/3 mice; 6-OHDA = 0.86 [0.78, 0.94] ms, n = 26
786 neurons/3 mice, p = 0.84, MWU, Figure 7A, B). Moreover, in the presence of
787 intracellular BAPTA, PTNs neurons still show activity-dependent AP broadening in both
788 controls (1st AP = 0.78 [0.68, 0.86] ms, last AP = 1.14 [0.97, 1.24] ms, n = 17 neurons/3
789 mice, $p < 0.0001$, WSR, Figure 7C) and 6-OHDA mice (1st AP = 0.78 [0.73, 0.87] ms,
790 last AP = 1.14 [0.94, 1.33] ms, n = 16 neurons/3 mice, $p < 0.0001$, WSR, Figure 7C).
791 However, the extent of AP broadening during repetitive firing (10 spikes) was
792 comparable between groups (controls versus 6-OHDA mice, half-width of the 1st AP, p
793 = 0.5 between groups; half-width of the last AP, p = 0.8 between groups, MWU).
794 Further, the PTNs from both groups also showed similar intrinsic excitability in the
795 presence of BAPTA (Figure 7D). For example, the number of spikes at the maximal
796 current injection for controls = 38 [21, 55], while the value for 6-OHDA = 29 [18, 40], n =
797 26 neurons /3 mice for each group; p = 0.29, MWU test.

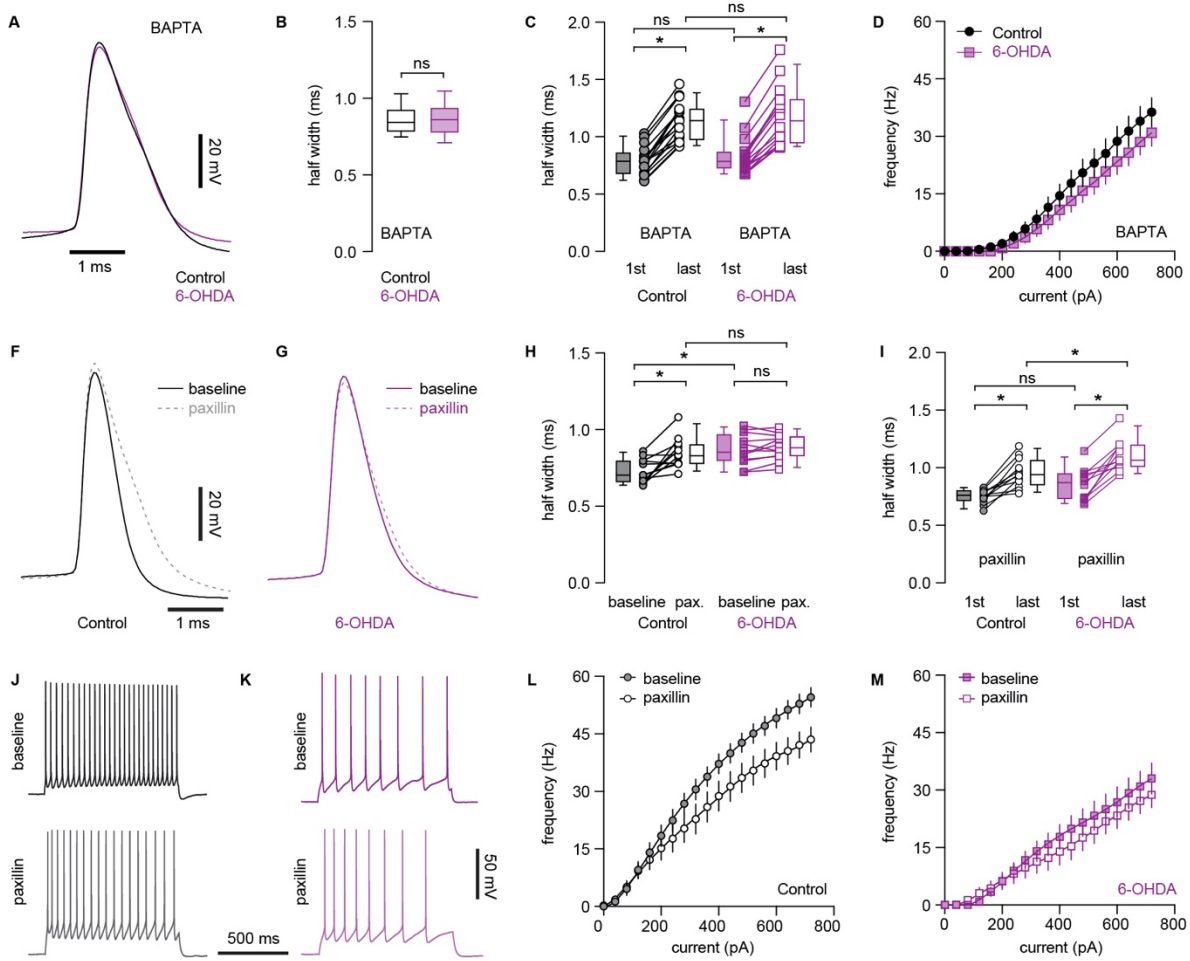

Figure 7. Decreased BK channel activity underlies AP broadening of PTNs following loss of midbrain DA neurons. A) Representative AP waveforms of PTNs from controls and 6-OHDA mice in the presence of BAPTA. APs were aligned at the threshold and overlaid for comparison. **B**) Boxplot showing AP width of PTNs at rheobase from controls and 6-OHDA mice in the presence of BAPTA. **C**) Boxplot showing AP broadening during repetitive firing of PTNs in controls and 6-OHDA mice in the presence of BAPTA. **D**) Frequency-current curve of PTNs in controls and 6-OHDA mice in the presence of BAPTA. **F and G**) Representative AP waveforms at rheobase before and after paxillin application in PTNs from controls (**F**) and 6-OHDA mice (**G**). APs were aligned at the threshold and overlaid for comparison. **H**) Summarized graph showing paxillin broadened APs of PTNs from both controls and 6-OHDA mice. **I**) Summarized graph showing AP broadening during repetitive firing of PTNs from controls and 6-OHDA mice in the presence of paxillin. **J-K**) Representative AP traces of PTNs from controls and 6-OHDA mice in the absence and presence of paxillin. L-M) Frequency-current curves showing paxillin decreased the frequency of PTNs firing om controls, but not in 6-OHDA mice. *, $p < 0.05$, WSR or MWU tests.

Next, we inhibited BK channel activity by a selective blocker paxillin (10 μM) and found that paxillin significantly decreased fAHP amplitude of PTNs in controls (baseline = 11.2 [7.7, 12.6] mV; paxillin = 8.3 [3.5, 10] mV, n = 12 neurons/3 mice, p = 0.005,

805 WSR), but not in 6-OHDA mice (baseline = 8.7 [7.3, 9.0] mV; paxillin = 8.7 [5.9, 9.8] mV,
806 n = 12 neurons/3 mice, WSR). Consistently paxillin significantly increased AP half-width
807 of PTNs at rheobase in controls (baseline = 0.7 [0.66, 0.79] ms, paxillin = 0.83 [0.78,
808 0.91] ms, n = 12 neurons/3 mice, p = 0.0024, WSR, Figure 7F, H), but not in 6-OHDA
809 mice (baseline = 0.85 [0.8, 0.97] ms, paxillin = 0.88 [0.83, 0.95] ms, n = 12 neurons/3
810 mice, p = 0.27, WSR, Figure 7G, H). Thus, blockade of BK channels by paxillin
811 abolished the difference in AP half-width of PTNs at rheobase in control and 6-OHDA
812 mice (AP half-width in paxillin, p = 0.22 between groups, MWU, Figure 7H). These
813 results suggests that BK channel activation contributes to AP repolarization and width of
814 PTNs in controls, but not in 6-OHDA mice.

815 Further, PTNs in 6-OHDA mice exhibited stronger activity-dependent AP
816 broadening during repetitive firing relative to those from controls (Figure 5D). However,
817 we found that inhibition of BK activity using paxillin abolished difference in the width of
818 the first AP of PTNs (the width of the first AP in paxillin, control = 0.76 [0.71, 0.8] ms, 6-
819 OHDA = 0.87 [0.73, 0.95] ms, p = 0.1, MWU, Figure 7I), but did not affect the robust AP
820 broadening during repetitive firing in 6-OHDA mice relative to that in controls (the width
821 of the last AP in paxillin, control = 0.94 [0.85, 1.06] ms, 6-OHDA = 1.06 [1.0, 1.2] ms, p
822 = 0.01, n = 12 neurons/3 mice for each group, Figure 7I). These results suggest that an
823 unidentified ionic conductance, other than BK channels, also contributes to the activity-
824 dependent AP broadening of PTNs in both controls and 6-OHDA mice, which may play
825 a dominant role in parkinsonian state.

826 Last, we tested whether BK channel dysfunction contributes to the impaired
827 excitability of PTNs in parkinsonism. In agreement with its role in AP repolarization,

851 blockade of BK channels by paxillin decreased the excitability of PTNs in controls (spike
852 numbers at the maximal current injection, baseline = 55 [49, 59], paxillin = 44 [36, 55], n
853 = 12 neurons/3 mice, p = 0.0015, WSR, Figure 7J, L), but not in 6-OHDA mice (baseline
854 = 37 [20, 47], paxillin = 30 [21, 40], n = 12 neurons/3 mice, p = 0.12, WSR, Figure 7K,
855 M). However, paxillin did not abolish the difference in the firing frequency of PTNs
856 between groups (maximal firing frequency, before paxillin p = 0.0002 between groups,
857 after paxillin, p = 0.0047, MWU), suggesting BK channels dysfunction partially
858 contributes to the decreased intrinsic excitability of PTNs in parkinsonism.
859
860 **DA cannot recue the decreased intrinsic excitability of PTNs in parkinsonism**
861 M1 receives dopaminergic inputs from the ventral tegmental area and these neurons
862 are partially degenerate in 6-OHDA mice (Hosp et al., 2011, 2015; Hosp and Luft, 2013).
863 Next, we tested whether a disrupted mesocortical DA neuromodulation contributes to
864 the intrinsic adaptations of PTNs in M1. DA receptors on PTNs were activated through
865 bath perfusion of DA (10 μM). However, activation of DA receptors produced negligible
866 effects to the intrinsic excitability of M1 PTNs in controls (e.g., the maximal firing
867 frequency, baseline = 56 [50, 60] Hz; DA = 59 [43, 63] Hz; n = 10 neurons/3 mice; p =
868 0.9, WSR; Figure. 8A, C, E). In addition, application of DA (10 μM) did not produce
869 significant effects to the intrinsic excitability of M1 PTNs in 6-OHDA mice either (e.g.,
870 the maximal firing frequency, baseline = 37 [34, 47] Hz, DA = 39 [35, 45] Hz, n = 12
871 neurons/3 mice; p = 0.7, WSR; Figure 8B-E). Further, we found that DA (10 μM) did not
872 alter the AP width of PTNs in both groups either (controls: baseline = 0.7 [0.63, 0.74]
873 ms, DA = 0.7 [0.62, 0.73] ms, n = 10 neurons/3 mice, p = 0.77, WSR; 6-OHDA: baseline

= 0.78 [0.71, 0.82] ms, 6-OHDA DA = 0.79 [0.67, 0.87] ms, n = 12 neurons/3 mice, p = 0.8, WSR, Figure 8F). These data suggested that restoration of local DA neuromodulation cannot rescue the impaired intrinsic excitability and AP broadening of M1 PTNs following the loss of midbrain DA neurons.

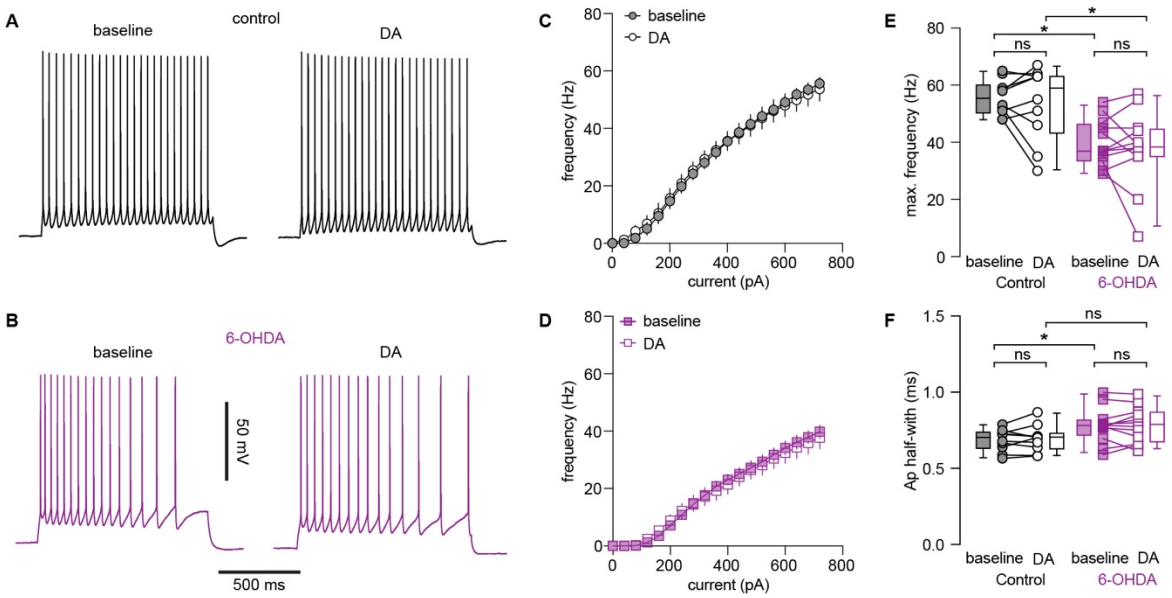

Figure 8. DA application could not rescue the decreased excitability of PTNs following loss of midbrain DA neurons. **A-B**) Representative AP traces of PTNs from controls and 6-OHDA mice in the absence and presence of DA. **C-D**) Frequency-current curves of PTNs from controls (C) and 6-OHDA mice (D) in the absence and presence of DA. **E**) Summarized graphs showing the lack of impact of DA on maximal firing frequency of PTNs from controls and 6-OHDA mice. **F**) Summarized graphs showing the lack of impact of DA on AP width of PTNs from controls and 6-OHDA mice *, $p < 0.05$, WSR or MWU tests.

907 **Discussion**

908 We studied changes in the intrinsic properties of M1 pyramidal neurons in
909 experimental parkinsonism. We found a cell-type-specific decrease of the intrinsic
910 excitability of M1 PTNs, but not the ITNs, in parkinsonism. We demonstrated that
911 impaired persistent Na^+ channel function led to an elevated AP threshold and played a
912 major role in the decreased intrinsic excitability of M1 PTNs. In addition, M1 PTNs also
913 exhibited broadened APs, which partially contributes to the decreased excitability of
914 PTNs during repetitive firing. Further, we revealed that impaired BK channel function
915 underlies the broadened APs of M1 PTNs in parkinsonism. Last, we showed that the
916 decreased intrinsic excitability of M1 PTNs were not reversible by the acute activation of
917 dopaminergic receptors. Our findings strongly suggest that the loss of midbrain DA
918 neurons not only alters basal ganglia activity, but also triggers intrinsic adaptations in
919 M1 circuitry, which contribute to the pathophysiology of parkinsonism.

920 Cell-type-specific changes in spontaneous activity of M1 pyramidal neurons were
921 first reported in MPTP-treated primates by Pasquereau and Turner (2011). In their
922 excellent work, the authors demonstrated a decreased firing rate and an increased firing
923 irregularity of spontaneous activity of antidromically identified PTNs; in contrast, the
924 firing rate and pattern of corticostriatal neurons were largely intact in MPTP-treated
925 monkeys (Pasquereau and Turner, 2011). Given the different anatomical projections
926 and function of M1 neuron subtypes in motor control, these subtype-specific changes in
927 neuronal activity have great implications in understanding of pathophysiology of
928 parkinsonian motor signs. Yet, few studies have been conducted to understand the
929 cellular and synaptic mechanisms underlying those changes in M1 neuronal activities in

954 parkinsonism. To address this question, we employed *ex vivo* electrophysiology to study
955 the intrinsic properties of projection-defined M1 pyramidal neurons in parkinsonism.
956 Following chronic midbrain DA degeneration, PTNs, but not the ITNs, in the L5b of M1
957 showed decreased intrinsic excitability and this finding is consistent with the earlier
958 findings in MPTP-treated primates (Pasquereau and Turner, 2011). Given the innervation
959 of subcortical motor centers by M1 PTNs, these results suggested that intrinsic
960 adaptations of M1 pyramidal neurons contribute to an insufficient motor cortical outputs
961 in parkinsonism, in addition to an elevated basal ganglia inhibition as proposed by the
962 classical model (Albin et al., 1989; DeLong, 1990; Galvan and Wichmann, 2008). Thus we
963 propose that these adaptations are important aspects of pathophysiology of
964 parkinsonism.

965 The decreased excitability of PTNs in 6-OHDA mice associated with a
966 depolarized AP threshold and could be normalized by I_{NaP} blockade using low
967 concentration of TTX. These results, together with the disrupted AP rising kinetics of
968 PTNs in 6-OHDA mice, suggest that an impaired I_{NaP} function decreases the availability
969 of Na_T channels that underlie AP depolarization and further promotes their inactivation
970 during repetitive firing, leading to the decreased excitability of PTNs. We posit that the
971 decreased intrinsic excitability makes neurons are more sensitive to synaptic inputs, as
972 that occurs in basal ganglia neurons in parkinsonism (Wilson 2013). Thus, it is likely that
973 the increased bursting pattern of activity of PTNs *in vivo* can be largely triggered by
974 synaptic inputs, but the enhanced spike adaptation leads to a reduced intraburst
975 frequency in MPTP-treated monkeys (Pasquereau and Turner, 2011; Pasquereau et al.,

1004 2016). Further studies will be needed to determine how synaptic inputs shape M1
1005 neuronal activity in parkinsonism.

1006 APs were significantly broadened in PTNs of parkinsonian animals (Figures 4A,
1007 5A, 5B). AP width has significant impact on Ca^{2+} influx during APs (Bean, 2007), yet
1008 functional implications of AP broadening in intracellular Ca^{2+} dynamics remain unknown.
1009 We showed that the AP broadening in PTNs in parkinsonism was occluded in the
1010 presence of BAPTA and paxillin, indicating a key role of BK channels in AP waveform
1011 modulation (Shao et al., 1999; Faber and Sah, 2003; Bean, 2007). It has been proposed that
1012 inactivation of BK channels could reduce Na_T availability for the subsequent AP
1013 generation during repetitive firing, leading to a decreased neuronal excitability (Bean,
1014 2007; Jaffe et al., 2011). Consistently, BK inhibition by paxillin strongly decreased
1015 excitability of PTNs in controls, but not in 6-OHDA mice, leading to a partial abolishment
1016 of the difference in neuronal excitability between groups (Figure 7L, 7M). Thus, we
1017 propose that impairments of both I_{NaP} and BK activities exacerbate progressive
1018 accumulation of Na_T inactivation during repetitive firing, leading to the decreased
1019 intrinsic excitability of PTNs in parkinsonism (Fleidervish et al., 1996). It is worthy to note
1020 that PTNs in both controls and 6-OHDA mice exhibited activity-dependent AP
1021 broadening in the presence of BK inhibition (Figures 7C, 7I). It indicates that unidentified
1022 ionic channels also contribute to AP repolarization of PTNs (Rudy and McBain, 2001;
1023 Pathak et al., 2016; Soares et al., 2017), and their inactivation underlies broadened APs in
1024 both groups, but possibly plays a major role in AP repolarization in parkinsonism.

1025 An acute application of DA did not affect the excitability of PTNs in both controls
1026 and in 6-OHDA mice. These results are consistent with recent findings that

1059 dopaminergic modulation of pyramidal neurons is mainly mediated indirectly by
1060 parvalbumin-expressing interneurons in M1 (Vitrac et al., 2014; Cousineau et al., 2020).
1061 Alternatively, it is possible that loss of mesocortical dopaminergic modulation
1062 contributes to the altered intrinsic excitability of PTNs, but such changes are not
1063 reversible by acute dopaminergic receptor activation. Compelling evidence suggests a
1064 critical role of dopaminergic modulation in the structural and functional plasticity of the
1065 motor cortical circuits (Lindenbach and Bishop, 2013; Ueno et al., 2014; Guo et al.,
1066 2015b). Last, circuitry mechanisms may also underlie cellular adaptions in M1 in
1067 parkinsonism. For example, recent studies highlighted a critical role of indirect pathway
1068 striatal projection neurons in driving cellular and synaptic adaptations in basal ganglia
1069 nuclei in parkinsonism, such as the subthalamic nucleus (Chu et al., 2017; Sharott et al.,
1070 2017; Ryan et al., 2018; McIver et al., 2019). Similarly, pathological basal ganglia outputs in
1071 parkinsonism can drive adaptive changes in M1 via the thalamocortical projections
1072 (Villalba et al., 2021).
1073 The exaggerated rhythmic activity and aberrant oscillations in the basal ganglia
1074 circuitry are closely related to the expression of motor symptoms in PD (Bevan et al.,
1075 2002; Little and Brown, 2014; Hemptinne et al., 2015). Indeed, the motor cortex exhibits
1076 abnormal neural activity in parkinsonian state at both the single-cell and population
1077 levels (Goldberg et al., 2002; Pasquereau and Turner, 2011; Hemptinne et al., 2015;
1078 Pasquereau et al., 2016). Both experimental and computation studies have indicated that
1079 cerebral cortical inputs play a crucial role in orchestrating pathological activity in basal
1080 ganglia nuclei (e.g., the external global pallidus and the subthalamic nucleus) (Bevan et
1081 al., 2002; Magill et al., 2004; Kita and Kita, 2011; Corbit et al., 2016; Chu et al., 2017; Sharott et

al., 2017). Recent studies also showed that electrical or optogenetic stimulation of the motor cortical pyramidal neurons and/or their projections produced therapeutic effects in parkinsonian animals (Gradinaru et al., 2009; Li et al., 2012; Sanders and Jaeger, 2016; Magno et al., 2019). Thus, an in-depth understanding of motor cortical adaptations in PD at the cellular and circuitry levels will help to design better therapeutic approaches with fewer off-target effects.

1112 **References cited:**

1113 Albin RL, Young AB, Penney JB (1989) The functional anatomy of basal ganglia
1114 disorders. Trends Neurosci 12:366–375.

1115 Barthas F, Kwan AC (2017) Secondary motor cortex: where 'sensory' meets 'motor' in
1116 the rodent frontal cortex. Trends Neurosci 40:181–193.

1117 Bean BP (2007) The action potential in mammalian central neurons. Nat Rev Neurosci
1118 8:451–465.

1119 Bevan MD, Magill PJ, Terman D, Bolam JP, Wilson CJ (2002) Move to the rhythm:
1120 oscillations in the subthalamic nucleus–external globus pallidus network. Trends
1121 Neurosci 25:525–531.

1122 Bodor ÁL, Giber K, Rovó Z, Ulbert I, Acsády L (2008) Structural correlates of efficient
1123 GABAergic transmission in the basal ganglia–thalamus pathway. J Neurosci 28:3090–
1124 3102.

1125 Chu H-Y, Atherton JF, Wokosin D, Surmeier DJ, Bevan MD (2015) Heterosynaptic
1126 regulation of external globus pallidus inputs to the subthalamic nucleus by the motor
1127 cortex. Neuron 85:364–376.

1128 Chu H-Y, McIver EL, Kovaleski RF, Atherton JF, Bevan MD (2017) Loss of hyperdirect
1129 pathway cortico-subthalamic inputs following degeneration of midbrain dopamine
1130 neurons. Neuron 95:1306-1318.e5.

1131 Contet C, Goulding SP, Kuljis DA, Barth AL (2016) BK channels in the central nervous
1132 system. Int Rev Neurobiol 128:281–342.

1133 Corbit VL, Whalen TC, Zitelli KT, Crilly SY, Rubin JE, Gittis AH (2016) Pallidostriatal
1134 projections promote β oscillations in a dopamine-depleted biophysical network model. J
1135 Neurosci 36:5556–5571.

1136 Cousineau J, Lescouzères L, Taupignon A, Delgado-Zabalza L, Valjent E, Baufreton J,
1137 Bon-Jégo ML (2020) Dopamine D2-like receptors modulate intrinsic properties and
1138 synaptic transmission of parvalbumin interneurons in the mouse primary motor cortex.
1139 Eneuro:ENEURO.0081-20.2020.

1140 DeLong MR (1990) Primate models of movement disorders of basal ganglia origin.
1141 Trends Neurosci 13:281–285.

1142 Deng P-Y, Klyachko VA (2016) Increased Persistent Sodium Current Causes Neuronal
1143 Hyperexcitability in the Entorhinal Cortex of Fmr1 Knockout Mice. Cell Reports
1144 16:3157–3166.

1145 Ebbesen CL, Brecht M (2017) Motor cortex — to act or not to act? Nat Rev Neurosci
1146 18:694–705.

1147 Ebbesen CL, Doron G, Lenschow C, Brecht M (2017) Vibrissa motor cortex activity
1148 suppresses contralateral whisking behavior. Nat Neurosci 20:82–89.

1149 Ebbesen CL, Insanally MN, Kopec CD, Murakami M, Saiki A, Erlich JC (2018) More
1150 than just a “motor”: recent surprises from the frontal cortex. J Neurosci 38:9402–9413.

1151 Economo MN, Viswanathan S, Tasic B, Bas E, Winnubst J, Menon V, Graybuck LT,
1152 Nguyen TN, Smith KA, Yao Z, Wang L, Gerfen CR, Chandrashekar J, Zeng H, Looger
1153 LL, Svoboda K (2018) Distinct descending motor cortex pathways and their roles in
1154 movement. Nature 563:79–84.

1155 Faber ESL, Sah P (2003) Ca2+-activated K+ (BK) channel inactivation contributes to
1156 spike broadening during repetitive firing in the rat lateral amygdala. J Physiol 552:483–
1157 497.

1158 Fieblinger T, Graves SM, Sebel LE, Alcacer C, Plotkin JL, Gertler TS, Chan CS,
1159 Heiman M, Greengard P, Cenci MA, Surmeier DJ (2014) Cell type-specific plasticity of
1160 striatal projection neurons in parkinsonism and L-DOPA-induced dyskinesia. Nat
1161 Commun 5:5316.

1162 Fleidervish IA, Friedman A, Gutnick MJ (1996) Slow inactivation of Na+ current and
1163 slow cumulative spike adaptation in mouse and guinea-pig neocortical neurones in
1164 slices. J Physiol 493:83–97.

1165 Galvan A, Wichmann T (2008) Pathophysiology of parkinsonism. Clin Neurophysiology
1166 Official J Int Fed Clin Neurophysiology 119:1459–1474.

1167 Gittis AH, Hang GB, LaDow ES, Shoenfeld LR, Atallah BV, Finkbeiner S, Kreitzer AC
1168 (2011) Rapid target-specific remodeling of fast–spiking inhibitory circuits after loss of
1169 dopamine. Neuron 71:858–868.

1170 Goldberg JA, Boraud T, Maraton S, Haber SN, Vaadia E, Bergman H (2002) Enhanced
1171 synchrony among primary motor cortex neurons in the 1-Methyl-4-Phenyl-1,2,3,6-
1172 Tetrahydropyridine primate model of Parkinson’s disease. J Neurosci 22:4639–4653.

1173 Gradinaru V, Mogri M, Thompson KR, Henderson JM, Deisseroth K (2009) Optical
1174 deconstruction of parkinsonian neural circuitry. Science 324:354–359.

1175 Guo J-Z, Graves AR, Guo WW, Zheng J, Lee A, Rodríguez-González J, Li N, Macklin
1176 JJ, Phillips JW, Mensh BD, Branson K, Hantman AW (2015a) Cortex commands the
1177 performance of skilled movement. Elife 4:e10774.

1178 Guo L, Xiong H, Kim J-I, Wu Y-W, Lalchandani RR, Cui Y, Shu Y, Xu T, Ding JB
1179 (2015b) Dynamic rewiring of neural circuits in the motor cortex in mouse models of
1180 Parkinson's disease. Nat Neurosci 18:1299–1309.

1181 Hemptinne C de, Swann NC, Ostrem JL, Ryapolova-Webb ES, Luciano MS,
1182 Galifianakis NB, Starr PA (2015) Therapeutic deep brain stimulation reduces cortical
1183 phase-amplitude coupling in Parkinson's disease. Nat Neurosci 18:779–786.

1184 Hosp JA, Luft AR (2013) Dopaminergic meso-cortical projections to M1: role in motor
1185 learning and motor cortex plasticity. Front Neurol 4:145.

1186 Hosp JA, Nolan HE, Luft AR (2015) Topography and collateralization of dopaminergic
1187 projections to primary motor cortex in rats. Exp Brain Res 233:1365–1375.

1188 Hosp JA, Pekanovic A, Rioult-Pedotti MS, Luft AR (2011) Dopaminergic projections
1189 from midbrain to primary motor cortex mediate motor skill learning. J Neurosci 31:2481–
1190 2487.

1191 Jaffe DB, Wang B, Brenner R (2011) Shaping of action potentials by type I and type II
1192 large-conductance Ca2+-activated K+ channels. Neuroscience 192:205–218.

1193 Kawai R, Markman T, Poddar R, Ko R, Fantana AL, Dhawale AK, Kampff AR, Ölveczky
1194 BP (2015) Motor cortex is required for learning but not for executing a motor skill.
1195 Neuron 86:800–812.

1196 Kita H, Kita T (2011) Cortical stimulation evokes abnormal responses in the dopamine-
1197 depleted rat basal ganglia. J Neurosci 31:10311–10322.

1198 Kress GJ, Yamawaki N, Wokosin DL, Wickersham IR, Shepherd GMG, Surmeier DJ
1199 (2013) Convergent cortical innervation of striatal projection neurons. Nat Neurosci
1200 16:665–667.

1201 Lee J, Wang W, Sabatini BL (2020) Anatomically segregated basal ganglia pathways
1202 allow parallel behavioral modulation. Nat Neurosci:1–11.

1203 Li Q, Ke Y, Chan DCW, Qian Z-M, Yung KKL, Ko H, Arbuthnott GW, Yung W-H (2012)
1204 Therapeutic deep brain stimulation in parkinsonian rats directly influences motor cortex.
1205 Neuron 76:1030–1041.

1206 Lindenbach D, Bishop C (2013) Critical involvement of the motor cortex in the
1207 pathophysiology and treatment of Parkinson's disease. Neurosci Biobehav Rev
1208 37:2737–2750.

1209 Little S, Brown P (2014) The functional role of beta oscillations in Parkinson's disease.
1210 Parkinsonism Relat D 20 Suppl 1:S44-8.

1211 Magill PJ, Sharott A, Bevan MD, Brown P, Bolam JP (2004) Synchronous unit activity
1212 and local field potentials evoked in the subthalamic nucleus by cortical stimulation. J
1213 Neurophysiol 92:700–714.

1214 Magno LAV, Tenza-Ferrer H, Collodetti M, Aguiar MFG, Rodrigues APC, Silva RS da,
1215 Silva J do P, Nicolau NF, Rosa DVF, Birbrair A, Miranda DM, Romano-Silva MA (2019)
1216 Optogenetic stimulation of the M2 cortex reverts motor dysfunction in a mouse model of
1217 Parkinson's disease. J Neurosci 39:3234–3248.

1218 Mallet N, Pogosyan A, Sharott A, Csicsvari J, Bolam JP, Brown P, Magill PJ (2008)
1219 Disrupted dopamine transmission and the emergence of exaggerated beta oscillations
1220 in subthalamic nucleus and cerebral cortex. J Neurosci 28:4795–4806.

1221 Mathai A, Ma Y, Paré J-F, Villalba RM, Wichmann T, Smith Y (2015) Reduced cortical
1222 innervation of the subthalamic nucleus in MPTP-treated parkinsonian monkeys. Brain
1223 138:946–962.

1224 McGregor MM, Nelson AB (2019) Circuit mechanisms of Parkinson's disease. Neuron
1225 101:1042–1056.

1226 McIver EL, Atherton JF, Chu H-Y, Cosgrove KE, Kondapalli J, Wokosin D, Surmeier DJ,
1227 Bevan MD (2019) Maladaptive downregulation of autonomous subthalamic nucleus
1228 activity following the loss of midbrain dopamine neurons. Cell Reports 28:992-1002.e4.

1229 Milescu LS, Yamanishi T, Ptak K, Smith JC (2010) Kinetic Properties and Functional
1230 Dynamics of Sodium Channels during Repetitive Spiking in a Slow Pacemaker Neuron.
1231 J Neurosci 30:12113–12127.

1232 Oswald MJ, Tantirigama MLS, Sonntag I, Hughes SM, Empson RM (2013) Diversity of
1233 layer 5 projection neurons in the mouse motor cortex. Front Cell Neurosci 7:174.

1234 Parker JG, Marshall JD, Ahanonu B, Wu Y-W, Kim TH, Grewe BF, Zhang Y, Li JZ, Ding
1235 JB, Ehlers MD, Schnitzer MJ (2018) Diametric neural ensemble dynamics in
1236 parkinsonian and dyskinetic states. Nature 557:177–182.

1237 Parker PRL, Lalive AL, Kreitzer AC (2016) Pathway-specific remodeling of
1238 thalamostriatal synapses in parkinsonian mice. Neuron 89:734–740.

1239 Pasquereau B, DeLong MR, Turner RS (2016) Primary motor cortex of the parkinsonian
1240 monkey: altered encoding of active movement. Brain 139:127–143.

1241 Pasquereau B, Turner RS (2011) Primary motor cortex of the parkinsonian monkey:
1242 differential effects on the spontaneous activity of pyramidal tract-type neurons. Cereb
1243 Cortex 21:1362–1378.

1244 Pathak D, Guan D, Foehring RC (2016) Roles of specific Kv channel types in
1245 repolarization of the action potential in genetically identified subclasses of pyramidal
1246 neurons in mouse neocortex. J Neurophysiol 115:2317–2329.

1247 Rudy B, McBain CJ (2001) Kv3 channels: voltage-gated K+ channels designed for high-
1248 frequency repetitive firing. Trends Neurosci 24:517–526.

1249 Ryan MB, Bair-Marshall C, Nelson AB (2018) Aberrant striatal activity in parkinsonism
1250 and levodopa-induced dyskinesia. Cell Reports 23:3438-3446.e5.

1251 Sanders TH, Jaeger D (2016) Optogenetic stimulation of cortico-subthalamic projections
1252 is sufficient to ameliorate bradykinesia in 6-ohda lesioned mice. Neurobiol Dis 95:225–
1253 237.

1254 Sauerbrei BA, Guo J-Z, Cohen JD, Mischiati M, Guo W, Kabra M, Verma N, Mensh B,
1255 Branson K, Hantman AW (2020) Cortical pattern generation during dexterous
1256 movement is input-driven. Nature 577:386–391.

1257 Shao L, Halvorsrud R, Borg-Graham L, Storm JF (1999) The role of BK-type Ca2+-
1258 dependent K+ channels in spike broadening during repetitive firing in rat hippocampal
1259 pyramidal cells. J Physiol 521:135–146.

1260 Sharott A, Vinciati F, Nakamura KC, Magill PJ (2017) A population of indirect pathway
1261 striatal projection neurons is selectively entrained to parkinsonian beta oscillations. J
1262 Neurosci 37:9977–9998.

1263 Sheets PL, Suter BA, Kiritani T, Chan CS, Surmeier DJ, Shepherd GMG (2011)
1264 Corticospinal-specific HCN expression in mouse motor cortex: I h -dependent synaptic
1265 integration as a candidate microcircuit mechanism involved in motor control. J
1266 Neurophysiol 106:2216–2231.

1267 Shen W, Plotkin JL, Francardo V, Ko WKD, Xie Z, Li Q, Fieblinger T, Wess J, Neubig
1268 RR, Lindsley CW, Conn PJ, Greengard P, Bezard E, Cenci MA, Surmeier DJ (2015) M4
1269 muscarinic receptor signaling ameliorates striatal plasticity deficits in models of L-
1270 DOPA-induced dyskinesia. Neuron 88:762–773.

1271 Shepherd GMG (2013) Corticostriatal connectivity and its role in disease. Nat Rev
1272 Neurosci 14:278–291.

1273 Shimamoto SA, Ryapolova-Webb ES, Ostrem JL, Galifianakis NB, Miller KJ, Starr PA
1274 (2013) Subthalamic nucleus neurons are synchronized to primary motor cortex local
1275 field potentials in Parkinson's disease. J Neurosci 33:7220–7233.

1276 Soares D, Goldrick I, Lemon RN, Kraskov A, Greensmith L, Kalmar B (2017)
1277 Expression of Kv3.1b potassium channel is widespread in macaque motor cortex

1278 pyramidal cells: A histological comparison between rat and macaque. J Comp Neurol
1279 525:2164–2174.

1280 Sreenivasan V, Esmaeili V, Kiritani T, Galan K, Crochet S, Petersen CCH (2016)
1281 Movement initiation signals in mouse whisker motor cortex. Neuron 92:1368–1382.

1282 Suter BA, Migliore M, Shepherd GMG (2013) Intrinsic electrophysiology of mouse
1283 corticospinal neurons: a class-specific triad of spike-related properties. Cereb Cortex
1284 23:1965–1977.

1285 Ueno T, Yamada J, Nishijima H, Arai A, Migita K, Baba M, Ueno S, Tomiyama M (2014)
1286 Morphological and electrophysiological changes in intratelencephalic-type pyramidal
1287 neurons in the motor cortex of a rat model of levodopa-induced dyskinesia. Neurobiol
1288 Dis 64:142–149.

1289 Viaro R, Morari M, Franchi G (2011) Progressive motor cortex functional reorganization
1290 following 6-hydroxydopamine lesioning in rats. J Neurosci 31:4544–4554.

1291 Vila M, Périer C, Féger J, Yelnik J, Faucheux B, Ruberg M, Raisman-Vozari R, Agid Y,
1292 Hirsch EC (2000) Evolution of changes in neuronal activity in the subthalamic nucleus of
1293 rats with unilateral lesion of the substantia nigra assessed by metabolic and
1294 electrophysiological measurements. Eur J Neurosci 12:337–344.

1295 Villalba RM, Behnke JA, Pare J-F, Smith Y (2021) Comparative Ultrastructural Analysis
1296 of Thalamocortical Innervation of the Primary Motor Cortex and Supplementary Motor
1297 Area in Control and MPTP-Treated Parkinsonian Monkeys. Cereb Cortex New York N Y
1298 1991.

1299 Villalobos C, Shakkottai VG, Chandy KG, Michelhaugh SK, Andrade R (2004) SKCa
1300 channels mediate the medium but not the slow calcium-activated afterhyperpolarization
1301 in cortical neurons. J Neurosci 24:3537–3542.

1302 Vitrac C, Péron S, Frappé I, Fernagut P-O, Jaber M, Gaillard A, Benoit-Marand M
1303 (2014) Dopamine control of pyramidal neuron activity in the primary motor cortex via D2
1304 receptors. Front Neural Circuit 8:13.

1305 Wang X, Liu Y, Li X, Zhang Z, Yang H, Zhang Y, Williams PR, Alwahab NSA, Kapur K,
1306 Yu B, Zhang Y, Chen M, Ding H, Gerfen CR, Wang KH, He Z (2017) Deconstruction of
1307 corticospinal circuits for goal-directed motor skills. Cell 171:440-455.e14.

1308 Willard AM, Isett BR, Whalen TC, Mastro KJ, Ki CS, Mao X, Gittis AH (2019) State
1309 transitions in the substantia nigra reticulata predict the onset of motor deficits in models
1310 of progressive dopamine depletion in mice. Elife 8:e42746.

1311